European Journal of Pharmaceutics and Biopharmaceutics 207 (2025) 114619

Contents lists available at ScienceDirect

European Journal of Pharmaceutics and Biopharmaceutics

journal homepage: www.elsevier.com/locate/ejpb

Stearic acid-capped mesoporous silica microparticles as novel needle-like-structured drug delivery carriers

Mohamad Anas Al Tahan [a,b], Ali Al-Khattawi [a,*], Craig Russell [a,*]

[a] School of Pharmacy, College of Health and Life Sciences, Aston University, Birmingham, United Kingdom
[b] Aston Medical Research Institute, College of Health and Life Sciences, Aston University, Birmingham, United Kingdom

ARTICLE INFO

Keywords:
Mesoporous silica microparticles
Stearic acid
Capping
Needles
Autofluorescence
Crystals

ABSTRACT

Mesoporous silica are widely utilised as drug carriers due to their large pore volume and surface area, which facilitate effective loading. Additionally, they can be used to enhance drugs stability and protect against enzymatic degradation due to their silica framework. However, without the addition of a capping material, the loaded cargo may be prematurely released before reaching the target site. This work reports the functionalisation of a commercially available silica microparticle (SYLOID XDP 3050) with stearic acid at various stearic acid loading concentrations (20–120 % w/w). Scanning electron microscopy (SEM) analysis revealed that the pores were capped with stearic acid, with the filling ratio increasing proportionally to the loading concentration. Notably, needle-like structures appeared when the stearic acid amount exceeded 80 % w/w, surpassing the calculated theoretical maximum pore filling ratio (64.32 %). The molecular interactions were highlighted using Fourier-transform infrared spectroscopy (FTIR), as the intensity of the CH_3 increased with increased stearic acid loading concentrations. The needle-structures phenomenon was corroborated by 3D confocal imaging. It utilised the autofluorescence properties of stearic acid to demonstrate its presence within the carrier, with fluorescence intensity increasing alongside the stearic acid concentration. Differential scanning calorimetry (DSC) indicated the crystalline nature of these needle structures, which was further confirmed by X-ray diffraction (XRD) analysis, validating the crystallisation of the stearic acid needles. Moreover, nitrogen porosimetry was employed to assess the pore volume and surface area, where the formulation containing 120 % stearic acid exhibited the lowest pore volume (0.59 cc). This value was smaller than unloaded SYLOID (2.1 cc), indicating near-complete filling of the carrier. This newly developed SYLOID-stearic acid carrier will now be used to enhance formulation development as a platform to enhance protein oral drug delivery.

1. Introduction

Mesoporous silica are widely used as carriers for different materials as they possess adjustable porous structure, high loading capacity, and tuneable surface area, as well as relatively high silanol density [1]. The chemical stability of SiO_2 matrices, despite their non-biodegradable nature, makes the abundant pores in mesoporous silica ideal for accommodating various molecules. Their exceptional biocompatibility further supports applications in drug delivery, bioimaging, and biosensing, enabling safe and efficient interactions with biological systems [2]. In addition, mesoporous silica are employed for oral delivery and tailored for targeting purposes through the optimisation of their shape and surface properties. This can be achieved by surface modifications via numerous functional groups and active targeting [3]. Their rigid silica framework enhances drug stability, protecting sensitive therapeutics like proteins and peptides from enzymatic degradation and pH fluctuations, which improves bioavailability while minimising systemic toxicity [4]. Despite their advantages, mesoporous silica carriers may encounter challenges such as premature drug release before reaching the target site, making them susceptible to cellular uptake and potentially reducing the effectiveness of the carried active pharmaceutical ingredient (API). These drawbacks can be addressed using silica capping with the application of gatekeepers that control the pore opening and release of loaded materials through stimuli-responsive interactions [5,6]. The addition of gatekeepers such as peptides and lipids enhances the surface characteristics of silica particles, as some of these keepers are added to target a specific tissue or organ, enhancing the interaction with tissues [7,8]. There are several types and strategies for silica-capping, where

* Corresponding authors.
E-mail addresses: a.al-khattawi@aston.ac.uk (A. Al-Khattawi), c.russell6@aston.ac.uk (C. Russell).

https://doi.org/10.1016/j.ejpb.2024.114619
Received 28 October 2024; Received in revised form 9 December 2024; Accepted 20 December 2024
Available online 21 December 2024

lipids can be used as gatekeepers, and the cargo release mechanism is based on the oxidation and reduction of the lipid [9]. Additionally, using lipid-based materials as capping agents enables an easy surface functionalisation of the silica carrier with numerous ligands [10].

As mentioned above, mesoporous silica capping can be achieved using different materials, and one of the promising candidates is stearic acid [11]. According to the International Union of Pure and Applied Chemistry (IUPAC), stearic acid or octadecanoic acid is a long-chain saturated fatty acid containing 18 carbon atoms as in the molecular formula $C_{18}H_{36}O_2$, with a molar mass of 284.48 $g.mol^{-1}$. Stearic acid is highly biocompatible and possesses low cytotoxicity [12,13]. Like many lipid-based materials with a crystalline structure, stearic acid displays polymorphism. A case in which different crystal forms are constructed depending on the arrangements of molecules [14]. While there are four polymorphs of stearic acid, the majority of peer-reviewed literature typically refers to it as a three-polymorph material (A, B, and C). Polymorph C is often considered the most stable and is obtained through crystallisation with a polar solvent [15,16].

Stearic acid has been reported as a capping material for mesoporous silica nanoparticles (MSNs) to enhance drug delivery or change silica's properties [17]. An example is the incorporation of chitosan-stearic acid micelles with doxorubicin into MSNs [18]. There are several formulation techniques to incorporate stearic acid into mesoporous silica, including solvent evaporation. Santa Barbara 15 (SBA-15) mesoporous silica was used to construct stearic acid −SBA composites through ethanol solution impregnation to make SBA-15 retain the loaded cargo [19]. Another example of mesoporous silica-stearic acid complexes was investigated using tannic acid-MSNs to design a phase-changing material for energy storage and heat transfer applications [20]. Additionally, stearic acid has been reported to be used as a hydrophobic coating for MSNs to overcome the barriers to protein's oral delivery, considering that hydrophobic surfaces are preferred for better internalisation into the cells [21]. Functionalising MSNs with stearic acid can be helpful for drug delivery and interaction with cells, as it was found that lipids tend to enhance cellular penetration in a non-destructive manner [22]. However, despite the numerous advantages of MSNs, they face several drawbacks in regard to accumulation in tissues after oral ingestion due to their small size. Microparticles are superior to nanoparticles for drug delivery in specific contexts due to their localized action and minimal systemic effects [23,24]. Among these microparticles, is SYLOID, an amorphous porous microparticle, with an average pore size of 25 nm and a large surface area of 320 m^2/g [25]. Therefore, these properties make stearic acid and SYLOID XDP 3050 great candidates to construct a novel carrier for peptide delivery.

This study aims to create a novel lipid-mesoporous hybrid carrier for oral peptide delivery. This carrier will be made from a mesoporous carrier particle (SYLOID XDP 3050) and stearic acid via an ethanol evaporation method. This includes investigating stearic acid loading over a range of concentrations while characterising the morphology and size of the developed carrier using SEM imaging. In addition, DSC and laser diffraction will be used to confirm the crystal behaviour of stearic acid within SYLOID. Additionally, the autofluorescence properties of stearic acid will be used to detect its presence on the carrier's surface, while nitrogen porosimetry will be implemented to evaluate the pore volume and surface area changes with the increase in stearic acid concentration.

2. Materials and methods

2.1. Materials

Stearic acid with bulk density 400–500 kg/m^3 and ethanol absolute 99.8 % (HPLC grade) were purchased from Sigma-Aldrich (Dorset, UK). Mesoporous silica SYLOID ® XDP 3050 (average size of 59 μm, specific surface area of 310 m^2/g, average pore size of 25 nm, and pore volume of 1.74 cm^3/g) was kindly provided by W.R. Grace and Co (Worms, Germany).

2.2. Methods

2.2.1. Preparation of mesoporous SYLOID-stearic hybrid formulations

The SYLOID-stearic hybrid carrier was made using a modified ethanol evaporation method reported by Fan et al., where we reported modifications to the loading time and temperature [26]. Stearic acid was suspended in ethanol at concentrations ranging between 0.6 – 14 mg/ml and left on a magnetic stirrer while covered for 10 min at 25 °C until complete dissolution. SYLOID XDP 3050 was added to the stearic acid–ethanol solution and left to stir for 2 h at 25 °C while also being covered, where the amount of stearic acid to SYLOID ranged between 20–120 % w/w. These concentrations were chosen to systematically investigate its effect on the silica carrier morphological properties. This range was selected to ensure sufficient coverage at the lower end and to assess potential saturation or excess effects at the higher end. The suspension mixture was spattered on a watch glass and left to dry in a laboratory oven at 50 ℃ for 1 h. After drying, the samples were kept in glass vials for post-formulation characterisation.

2.2.2. Morphology of the hybrid SYLOID- lipid particles

The morphology of the particles was assessed via Scanning electron microscopy (SEM) imaging. The surface of the drug-loaded mesoporous silica particles was examined by Philips XL30 ESEM FEG (Hillsboro, OR, USA), operating at 10 kV under a high vacuum. Before SEM imaging, samples were coated with gold by a sputter coater. Approximately 1 mg of each sample was placed onto a double-sided adhesive strip on a sample holder. SEM images were captured at different magnifications.

2.2.3. Particle size analysis using laser diffraction

Sympatec laser diffraction (Sympatec, Germany) was used to determine the particle size of the formulations. The instrument was equipped with the vibratory feeder VIBRI, RODOS/L dispersion unit, and the compact laser diffraction sensor HELOS/BR. The used lens was the R3 Fourier lens (f = 100 mm) with a measuring range between 0.5–175 μm. The analysis parameters were as follows: PAQXOS 5.0 was employed as the software to analyse the results, the dispersion pressure was set to 1 bar, vacuum to 22 mbar, the feed rate as 50 %, and the optical concentration $\geq$ 1 %. All size analysis runs were done in triplicate for all formulations.

2.2.4. Thermal characterisation of silica-stearic formulations

The thermal properties of samples were characterised by the Differential Scanning Calorimetry DSC instrument TA Q200 (New Castle, DE, USA). Each sample was accurately weighed into a Tzero low-mass aluminium pan. The sample weight was 2.5 ± 0.1 mg, and the sample was heated in the range of 25–100 °C at a scanning rate of 10 °C/min under a nitrogen flow of 50 ml/min. Tzero low-mass pans and Tzero aluminium lids were used. TA universal analysis 2000 software (version 4.5) was employed to analyse the resulting DSC thermograms.

2.2.5. Fourier-transform infrared spectroscopy (FTIR) analysis

Investigation of molecular interactions was assessed using Nicolet™ iS™ 5 FTIR (Thermofisher, Waltham, USA) equipped with an ID5 diamond attenuated total reflectance (ATR) accessory. Before scanning, a background scan was collected, and approximately 30 mg of the powders were placed on the diamond plate. The spectrum was obtained by taking 36 scans in the region 500–3500 cm^{-1} at 4 cm^{-1} resolution. Atmospheric suppression and advanced ATR corrections were implemented after scanning. OMNIC™ was used for spectra analysis.

2.2.6. X-ray diffraction

XRD data were collected on a 3rd generation Malvern Panalytical Empyrean equipped with multicore (iCore/dCore) optics, providing Cu Kα1/2 radiation, and a Pixcel3D detector operating in 1D scanning mode

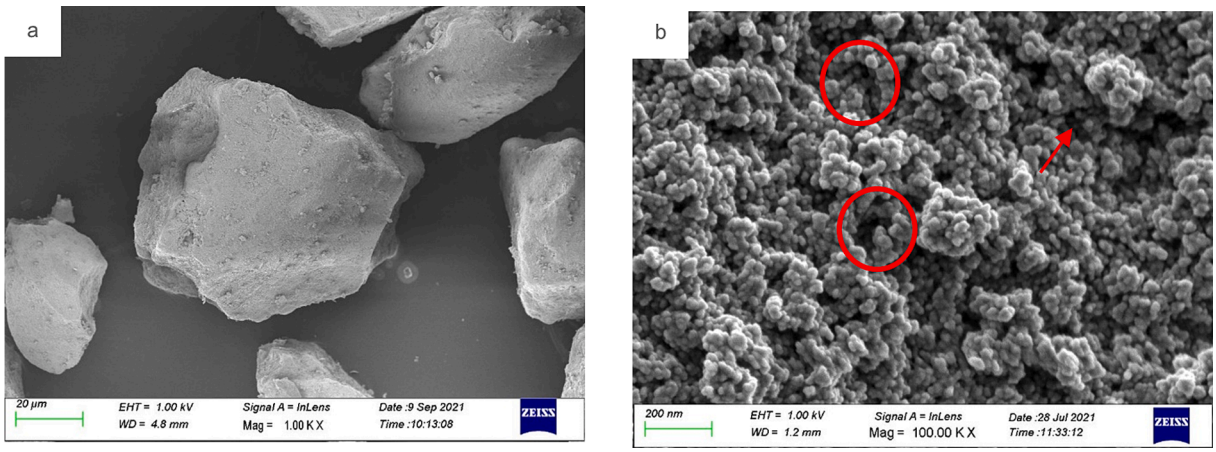

Fig. 1. SEM imaging of unloaded SYLOID XDP 3050 at different magnifications, presenting the particle morphology (a), and pores (b). The red circles and arrow identify the mesopores.

at a range between 5–65 2θ, step size of 0.05° and a count time of 1 s. For low-angle measurements, a beam knife was used to reduce the air scatter. Data were analysed using OriginPro 2021b software.

2.2.7. Helium pycnometry

The amorphous density of stearic acid was determined based on the method of Bavnhoj et al. [27]. Prior to analysis, the material was heated in a Heratherm oven (Thermo) at 10 ℃ above the melting point for 30 min, followed by quench cooling following the sample removal from the oven. The samples were grounded and weighed into the aluminium sample holder for analysis. A multipycnomter from Quantachrome Instruments (USA) was used for amorphous density determination, and the samples were purged with dry helium. Three consecutive measurements were taken, and the results are presented as mean ± SD.

2.2.8. Theoretical monolayer coverage and maximum pore loading calculation

The theoretical monolayer is the required amount of the adsorbate to cover the carrier in a monolayer coverage of the carrier (SYLOID) [28], and it can be calculated using the following equation:

$$X_m = \frac{SS_A \times 10^{20} \times Mw}{S_c \times N_A} \quad (1)$$

where X_m is the required stearic acid quantity to cover the adsorbate (SYLOID) in a monolayer (g/g), SS_A is the specific surface area of the adsorbate (m^2/g), Mw is the molecular weight of stearic acid (g/mol), S_c id the molecular surface area of the adsorbent ($Å^2$), and N_A is Avogadro's number. Another aspect to consider is the theoretical maximum pore loading it refers to the maximum theoretical amount of the material that is loaded into the porous carrier [29], and it can be calculated using the following equation:

$$TML = \left[\frac{V_p \times \rho_{stearic}}{1 + V_p \times \rho_{stearic}}\right] \times 100\% \quad (2)$$

where TML is the theoretical maximum load of the porous carrier, V_p is the pore volume of the silica carrier (cc/g), and $\rho_{stearic}$ is the true density of the loaded material (stearic acid).

2.2.9. Nitrogen porosimetry

The formulations ' specific surface area, pore volume, and pore size were determined using NOVAtouch LX2, Quantachrome instruments (Anton Parr, USA). Prior to analysis, samples were degassed for 18 h at 30 ℃. Specific surface area was acquired using standard BET (Brunauer, Emmett, Teller) model by means of Nitrogen adsorption at 1 bar nitrogen gas with a relative pressure p/p_0 in the range 0.05–0.3. Pore volume was determined using BJH (Barrett, Joyner, and Halenda) adsorption and BJH desorption methods. Kurk-Jaroniec-Sayari model [30] was used to calculate the pore size distribution of the carrier, considering that it is suitable for mesoporous silica carriers. Touchwin software (version 1.2 x) was used to retrieve data.

2.2.10. Fluorescence imaging

Confocal microscopy (TCS SP8, Leica Microsystems, GmbH) was used for imaging. A 405 nm diode laser and a white light laser at 70 % power were used to image fluorophores AlexaFluor 532. The excitation and emission wavelengths for stearic acid were 520–739 nm. HYD detectors were used for each channel, 20X dry APO lens was used for imaging, and all images were taken at 2048*2048 resolution with the imaging speed set at 200 Hz. The laser powers, gain, and emission wavelengths were kept consistent for quantification purposes. 3D image for the particle is generated, where the two planes are merged. For image analysis, LAS X 3.0 (Leica Microsystems GmbH) and Fiji [31] software applications were used.

2.2.11. Statistical analysis

Statistical analyses of data were performed with SPSS 28 program by using one-way Analysis of Variance (ANOVA) coupled with a Tukey post-hoc test. All experiments were conducted in triplicate. All data was presented as mean ± SD, and P-value < 0.05 is considered statistically significant.

3. Results and discussion

3.1. Morphology of the obtained hybrid SYLOID-lipid particles

The design of a novel mesoporous silica carrier with a needle-like formation of stearic acid on its surface commenced via investigating different stearic acid loading concentrations. Scanning electron microscopy (SEM) imaging was used to study and define the structure and morphological properties of the resulting stearic acid-capped SYLOID particles. SYLOID has a particle size of 59 µm, with an average pore size of 25 nm and a surface area of 320 m^2/g as reported in the literature [25,32]. The unloaded SYLOID particle structure and pores are highlighted in Fig. 1, where the red circles and arrow point.

To explore stearic acid effect on the porous structure of SYLOID after loading in different concentrations, images were taken at high magnifications for all formulations and presented in Fig. 2, while low magnification images were taken to check the particle's surface (Fig. 3). The silica pores seemed to be increasingly capped upon higher stearic acid loading, and nano-sized masses of stearic acid precipitated on the surface where the red arrows pointed. In formulations where loading is 100

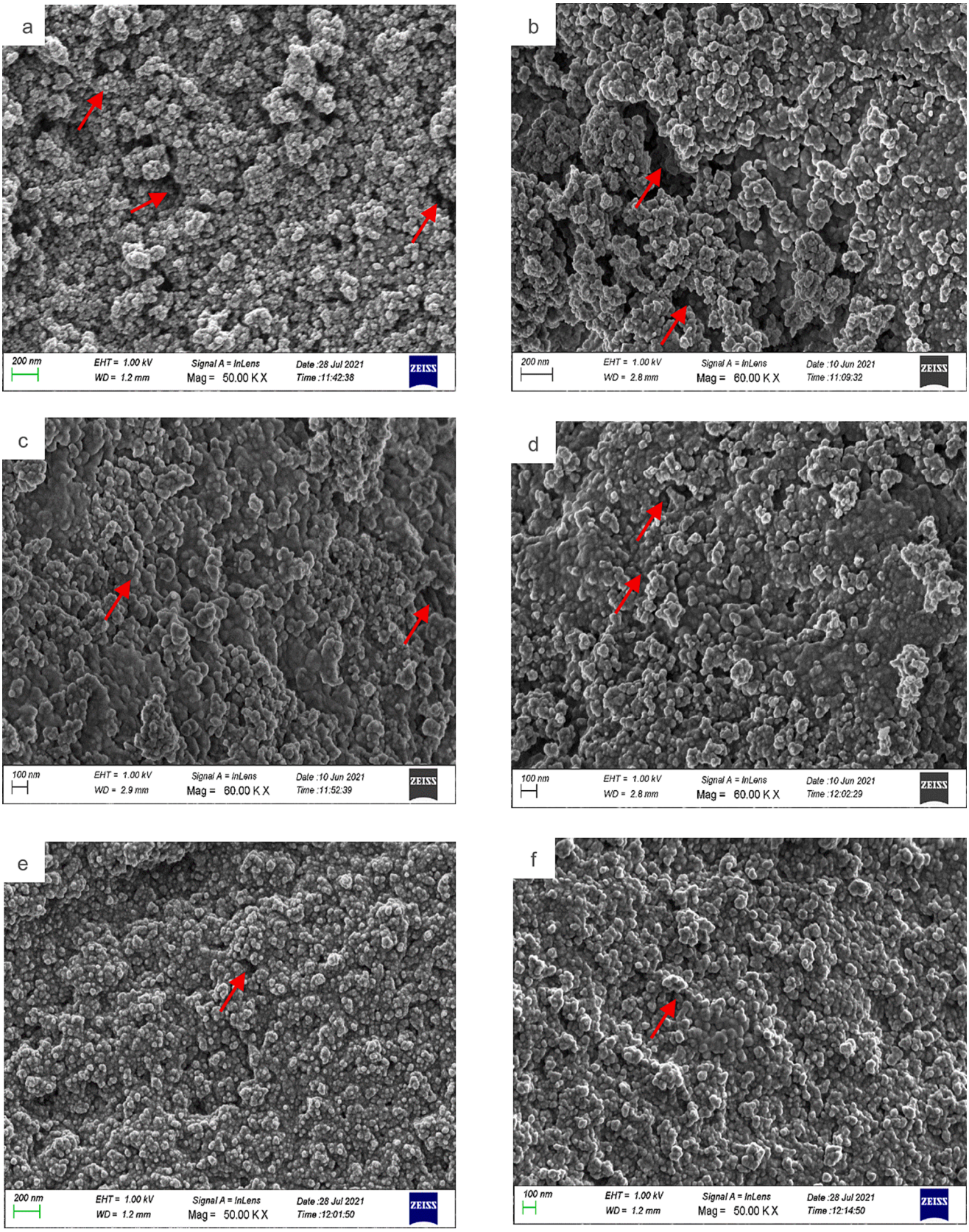

Fig. 2. High magnification SEM imaging for samples containing different stearic acid concentrations: 20% (a), 40% (b), 60% (c), 80% (d), 100% (e), and 120% (f). Red arrows identify mesopores that are capped with stearic acid increase.

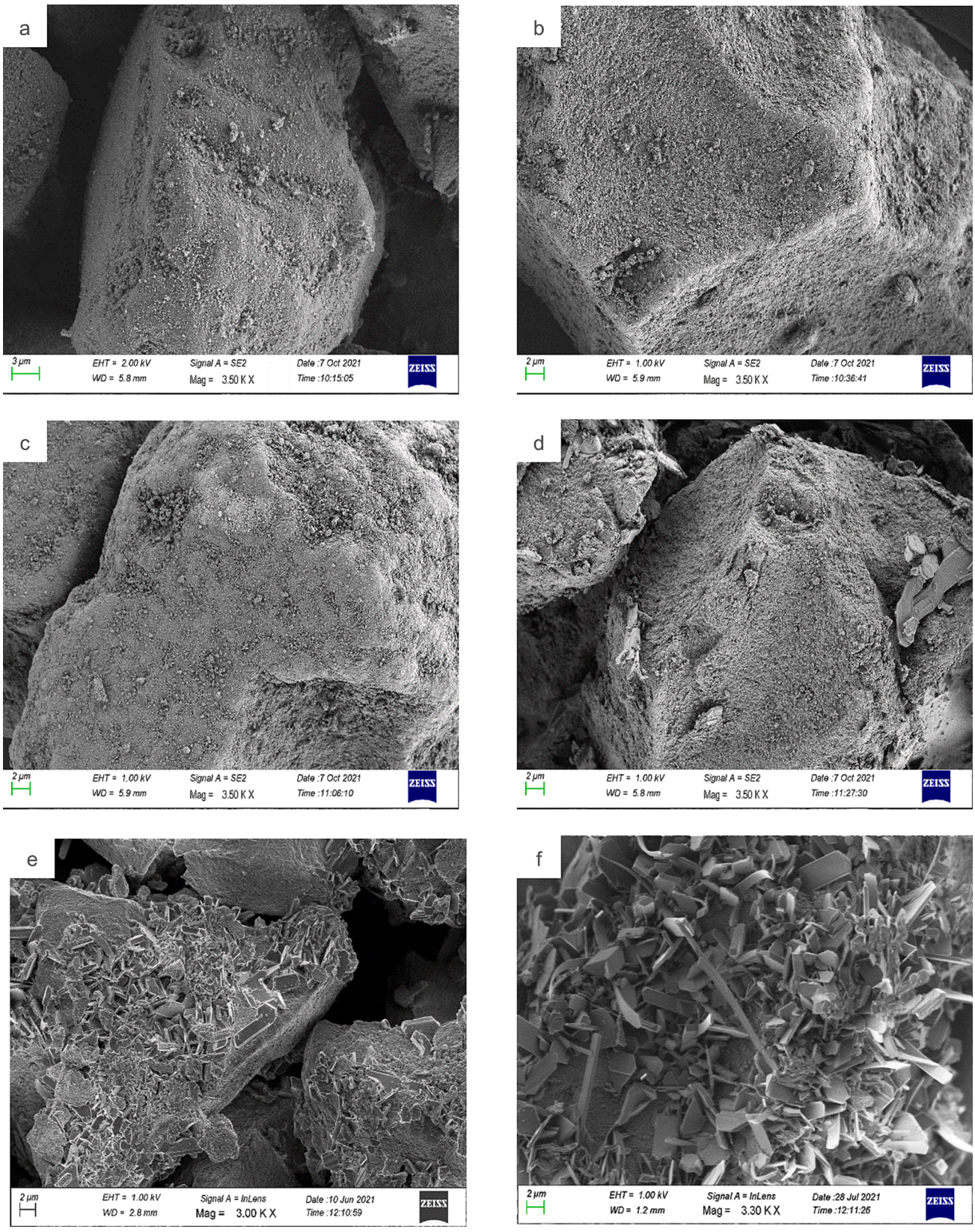

Fig. 3. Low magnification SEM surface imaging for SYLOID-stearic particles in different concentrations, where 20% (a), 40% (b), 60% (c), 80% (d), 100% (e), and 120% (f) focusing on the particle surface and identifying needle-like structures.

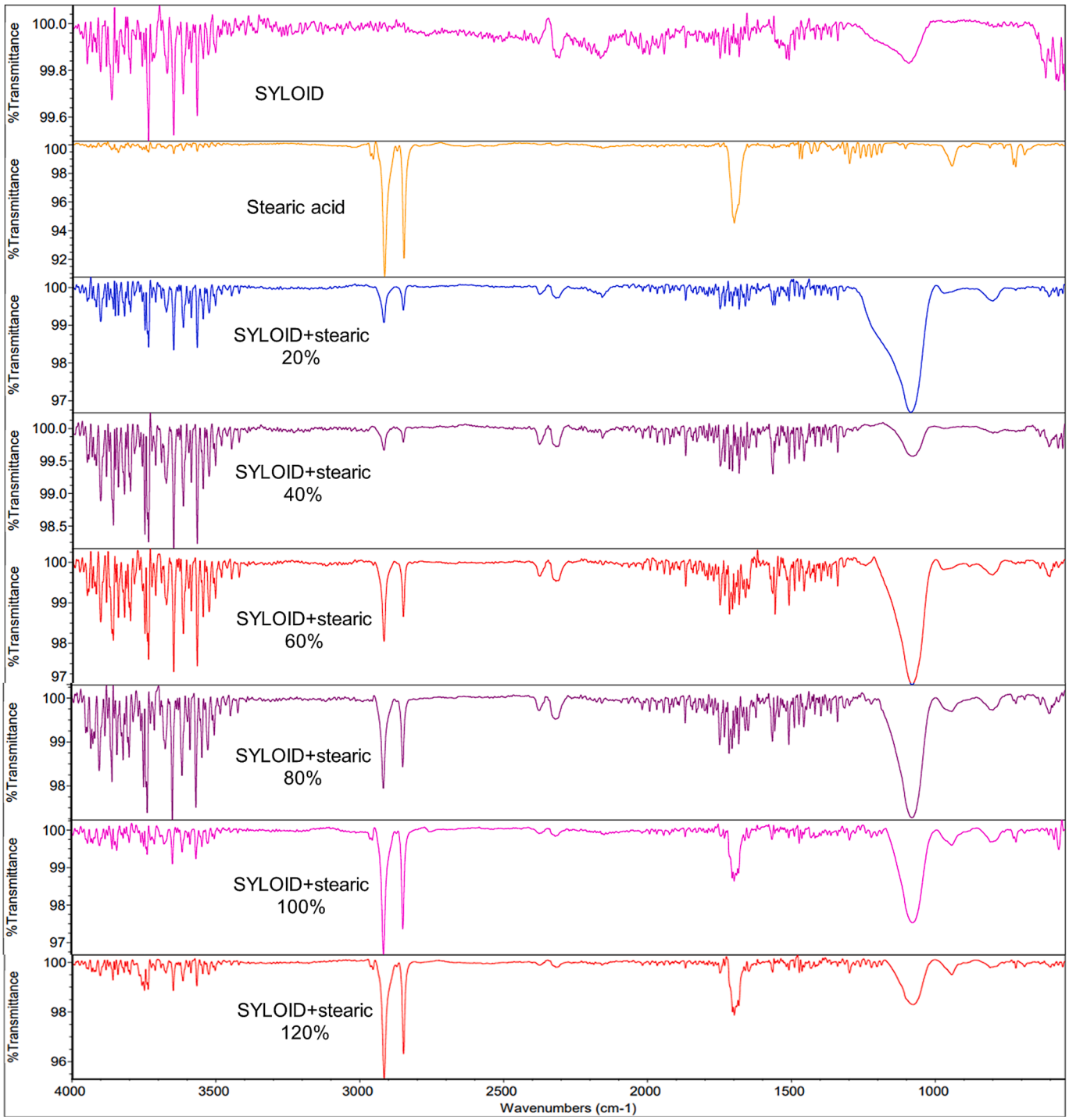

Fig. 4. FTIR profile for formulations containing different concentrations of stearic acid.

and 120 % w/w (Fig. 2 e-f), the pores appeared more capped with less prevalence of the darker areas representing less pore availability than formulations with less amounts of stearic acid (20–80 % w/w) as in (Fig. 2a-d). This could be attributed to the higher amounts of stearic acid, in which stearic acid nanoparticles occupied the pores and capped them. Even though the pores in (Fig. 2b) visually appear larger than the ones in (Fig. 2 a), this is related to the used carrier (SYLOID), being a non-ordered mesoporous silica microparticle that has a non-uniform pore distribution and sizes. As such, the visible appearance of the individual particles does not represent pore size distribution. This was evaluated using nitrogen porosimetry and reported in section 3.6.

As seen in Fig. 3 below, the surface of the silica carrier appeared highly similar to the unloaded SYLOID (Fig. 1 a) in the formulations that contained stearic acid in concentrations between 20–60 % w/w. However, when the amount increased to 80 %, small crystal-like structures were evident on the surface, even though they were not very apparent. However, when stearic acid concentration (w/w) increased to 100 %, needle-like structures started to appear on the surface of silica particles, which was attributable to stearic acid crystallisation (Fig. 3 e-f). These structures are consistent with stearic acid crystal habits observed in the literature [16], where needle-like formations are expected. According to the SEM investigations, this observation of needle-like morphologies at

concentrations exceeding 100 % was probably related to the capping of mesopores, as the two phenomena seem to coincide [17].

Furthermore, it can be observed that silica particles with higher stearic acid loading presented a more significant needle-like structure population area and larger crystals. This can be seen by comparing figure (3 e and 3f), where the amounts of stearic acid were 100 % and 120 %, respectively. When stearic acid was overloaded, in this case, more than 100 % w/w regarding the carrier, it blocked the pores or capped them, followed by the remaining stearic acid crystallising on the surface of the carrier.

The analogy of this would be a container filled to its total capacity, and the remaining liquid/material beyond capacity started to overflow. Stearic acid within pores was expected to be inhibited from significant crystallisation due to spatial confinement [33]. However, the excess on the surface was free to crystallise into large crystals. One possible hypothesis is the formation of nano stearic acid aggregates in the mesopores upon drying, as described below.

3.2. Theoretical minimum monolayer coverage and maximum pore loading

These stearic acid nanoparticles within the pores solidified and interconnected to close the pores. In contrast, the remaining stearic acid then used the near-surface nuclei of stearic acid to grow into directional needle-like shapes, similar to stearic acid and stearyl alcohol needle formations in oleogels [34]. It could be noticed that the stearic acid crystals were mostly perpendicular in their formation plane to that of the carrier surface. This constituted preliminary evidence supporting the notion that these crystals originated from the near-surface nuclei of stearic acid, as opposed to independently crystallising outside the carrier and subsequently adhering to it. If the latter were true, then most stearic acid particles would be seen lying flat on the surface of the carrier rather than perpendicular to it due to a preferable adhesion profile in that flat orientation.

To further support this finding, the theoretical amount for monolayer coverage and the theoretical maximum load of the carrier were calculated. These values are beneficial in presenting an idea of the theoretically required amount of the adsorbate to cover the carrier in a monolayer and the theoretical amount that will present a maximum pore loading [28].

The surface area of stearic acid was calculated using the largest two dimensions of the stearic acid molecule, which were 5.59 and 9.36 Å based on the short and long axis length [35], making a total theoretical molecular surface area of 52.32 $Å^2$. By applying Eq.(1) and assuming that the entire surface area of SYLOID was accessible for stearic adsorption, the stearic acid quantity for monolayer deposition was 0.2591 g/g. This amount meant that for achieving a theoretical monolayer coverage of SYLOID using stearic, the loading ratio would be 25.91 % (w/w). As for the theoretical maximum pore loading, by applying Eq.(2), the TML value was 64.32 %, which indicated that at a loading concentration of 64.32 % (w/w) of stearic acid, the theoretical maximum loading of the SYLOID pores could be potentially reached. The loading method could have affected the actual drug load of the carrier, where the slow evaporation of the loading solvent facilitated nucleation inside the pores of the carrier, occupying the pores in the process [36].

Even though formulations with low stearic acid amounts did not exhibit needle-like formations, stearic acid could still be located within the pores. FTIR analysis was conducted to investigate the presence of stearic acid in the different formulations. In addition, particle size distribution was assessed to determine the effects of stearic acid concentration on the size of the SYLOID-stearic hybrid particle.

3.3. FTIR analysis and particle sizing

As seen in Fig. 4 below, for the spectrum of SYLOID, a broad band at

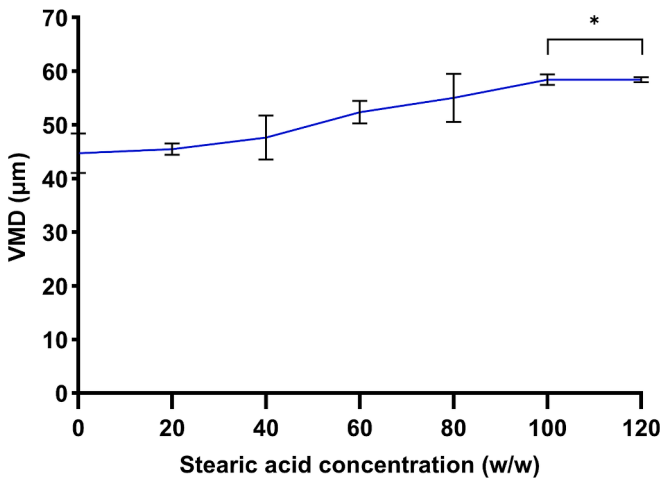

Fig. 5. The relationship between stearic acid concentration (X axis) and particle size mean (Y axis). Error bars represent standard deviation (n = 3) and (*) representing significant difference ($p < 0.05$).

1075 cm^{-1} corresponded to the asymmetric stretching of the siloxane group (Si-O-Si). In addition, the peaks at 800 cm^{-1} and 970 cm^{-1} corresponded to the symmetric stretching vibration of Si-O and Si-OH, respectively [37]. For the spectrum of stearic acid, the strong bands at 2850 and 2925 cm^{-1} were related to the symmetric and antisymmetric stretching of the methylene group, while the band at 1700 cm^{-1} was associated with the carboxylic group [38]. For the spectrum of SYLOID-stearic acid formulation, the intensity of the CH_3 group increased as the stearic acid amount in the formulation increased (20–120 %). Also, the carboxyl group intensity increased from 100 % stearic acid w/w. Additionally, the increased intensity is related to the presence of stearic acid inside the porous structure and on the surface. Furthermore, the intensity of the peak at 1075 cm^{-1} seemed to decrease with higher concentrations of stearic acid, indicating an interaction between the drug molecules and the negatively charged siloxane groups and forming bonds, which was reported previously with other drugs such as octreotide acetate [39].

To elaborate further on the effects of stearic acid's increased concentration on silica, particle size analysis was conducted using laser diffraction, which is presented in Fig. 5 below.

Indeed, the particle size of the prepared particles significantly increased (ANOVA, $p < 0.05$) as the amount of loaded stearic acid increased. The volume mean diameter (VMD) for the empty carrier (SYLOID) was 44.74 ± 3.36 µm, and has significantly increased to 58.41 ± 0.19 when the stearic acid amount was 120 % w/w. The increase in size could be related to the formation of needle-like structures on the surface of the particles. These needles could have increased the size of the carrier particles by an average of 14 µm, as seen in the above SEM images. To further support the presence of stearic acid needle-like structures at a specific concentration, confocal imaging was employed to detect stearic acid, considering its autofluorescence properties.

3.4. Confocal microscopy

Some lipids produce autofluorescence due to oxidation, absorbing long wavelengths and enabling fluorescence excitation across a broad spectral range [40]. For this reason, confocal microscopy was employed to highlight the presence of loaded stearic acid in the porous structure. Fig. 6 presents 3D-generated images for SYLOID-stearic formulations. SYLOID XDP 3050 is a non-fluorescent mesoporous carrier. However, as shown in figure (6 a-f), its surface exhibited minor fluorescence due to stearic acid (6 a). Increasing the stearic acid amount made the fluorescence more apparent (6 a-d). When the stearic acid exceeded 100 %, non-uniform needle-like structures appeared on the carrier's surface (6

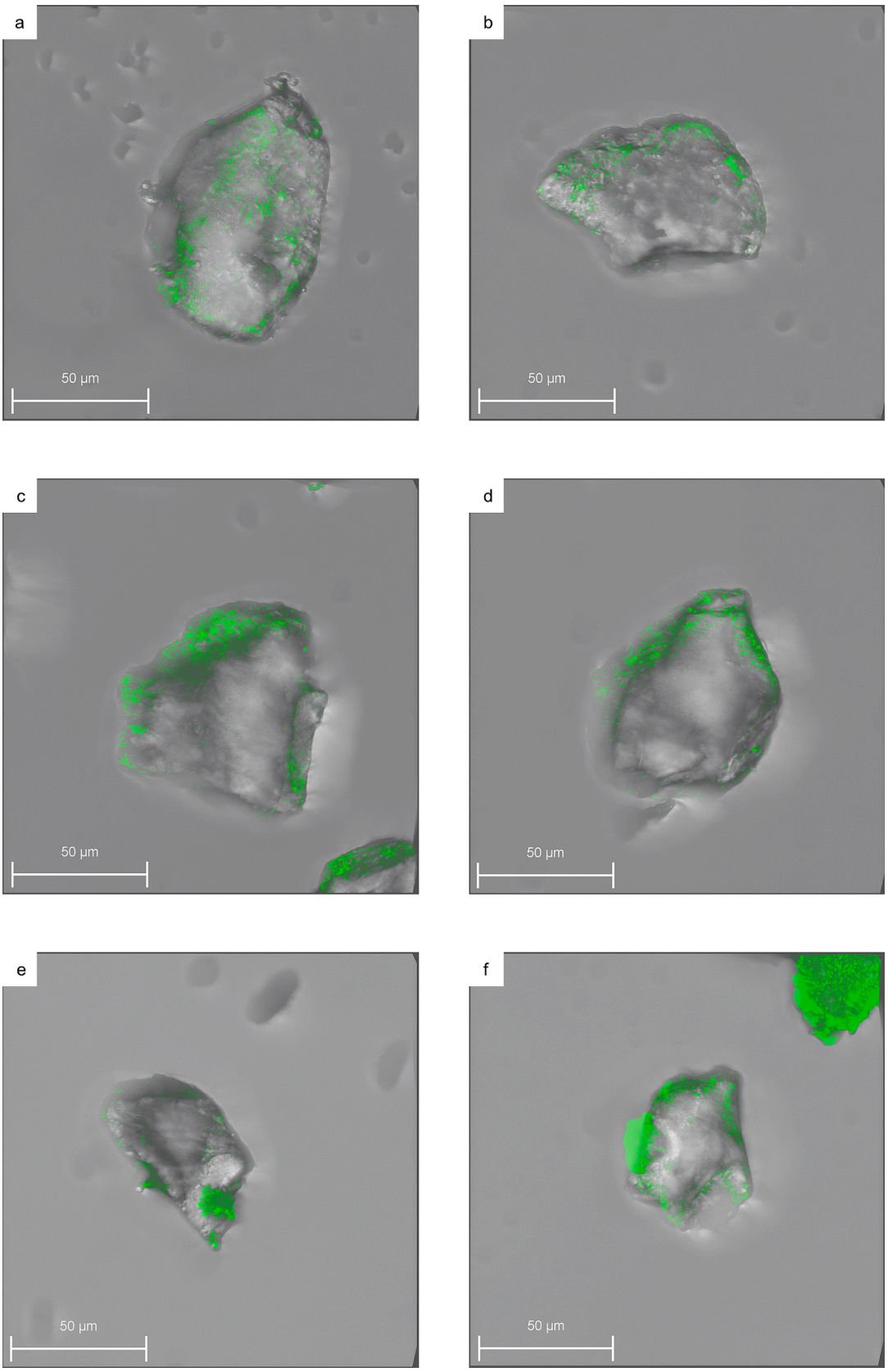

Fig. 6. 3D confocal imaging of SYLOID-stearic in different concentrations (w/w) showing stearic auto fluorescence; SYLOID-stearic 20% (a), SYLOID-stearic 40% (b), SYLOID-stearic 60% (c), SYLOID-stearic 80% (d), SYLOID-stearic 100% (e), SYLOID-stearic 120% (f).

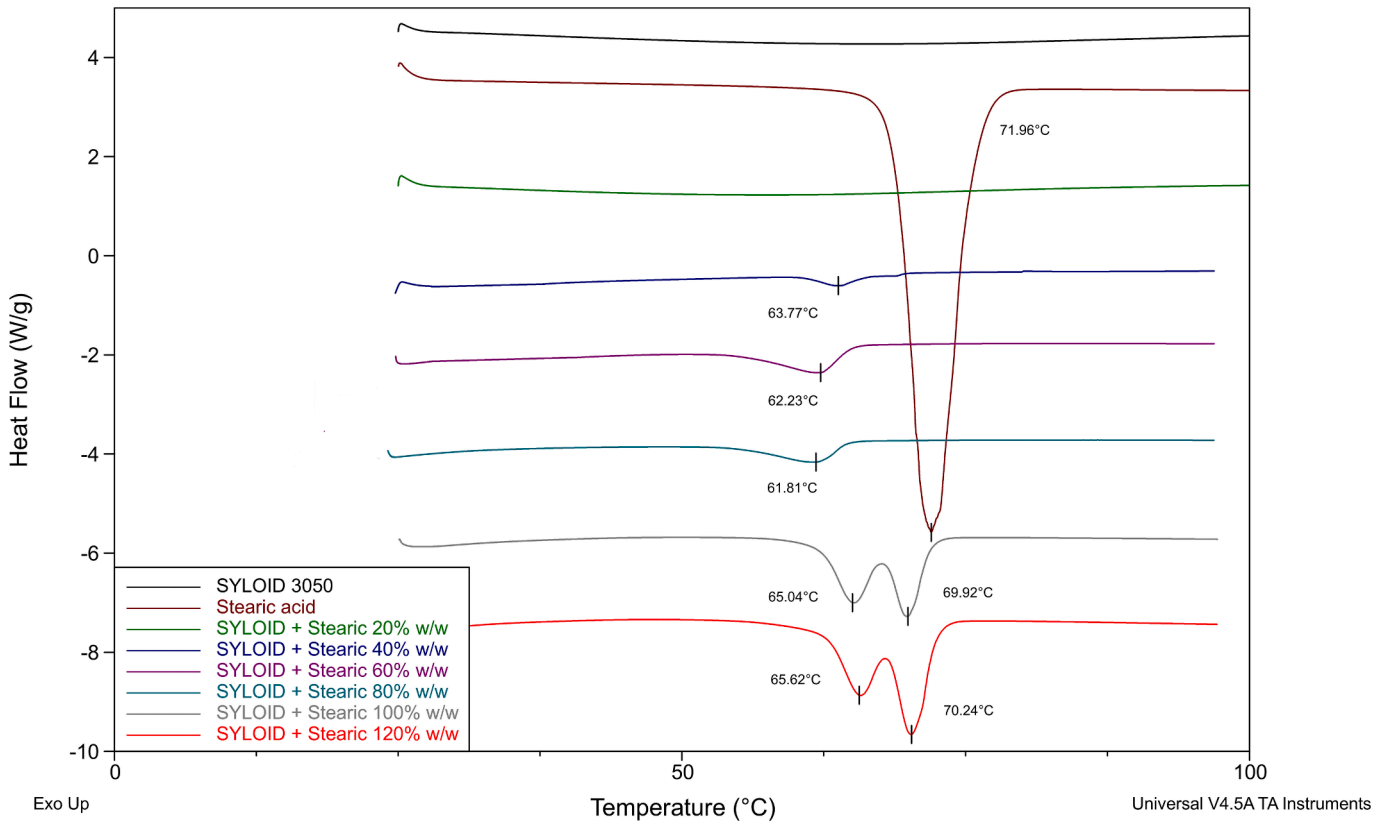

Fig. 7. DSC profile of SYLOID-stearic formulations in different concentrations identifying the melting points of stearic acid in its unloaded form and within SYLOID.

e). Further increases beyond 100 % enhanced fluorescence and crystallise clusters of fluorescent materials related to these needles (6f), supporting previous findings that higher concentrations of stearic acid (100 %) formed needle-like structures on SYLOID.

3.5. *Thermal and solid-state properties of SYLOID-stearic formulations*

DSC was used to investigate the loading and thermal properties of stearic acid within silica (Fig. 7). The DSC profiles were acquired at temperatures below 100 °C to avoid sublimation of stearic acid [41].

Stearic acid has three polymorphs, A, B, and C, with the C polymorph being the most stable [15,16]. Different polymorphs indicate potentially different physiochemical properties, including melting points [42]. In Fig. 7 above, stearic acid showed a melting point of 71.96 °C, which is similar to the melting point of pure C form (69.9 °C) previously reported in the literature [43,44].

According to FTIR results, the 20 % stearic acid-SYLOID formulation presented a characteristic peak of stearic acid but did not present an endothermic peak. This indicated either no presence of stearic acid in the formulation or low amounts. Upon increasing the percentage of stearic acid, an endothermic activity was evident, indicating the melting of stearic acid, and its intensity increased as the percentage of stearic acid increased within the formulation. Yet, the melting point was around 62 °C, which differed from stearic acid's (71.96 °C). This indicated that the loaded stearic acid within the carrier could be amorphous, considering SYLOID's ability to convert materials from the crystalline to amorphous form [45].

However, the endothermic peak became sharper and more apparent, seen in formulations containing 100 % and 120 %, indicating that the incorporated stearic acid could be in a crystalline form. This finding supported the SEM results, which showed crystal-like structures in formulations with stearic acid percentages exceeding 100 %. Moreover, the formulations containing 100 % and 120 % presented another endothermic activity with a melting point similar to stearic acid, indicating the presence of stearic acid in an amorphous form and crystal (needle-like structures). The second endothermic activity supported the observation in SEM results, where crystal-based needle-like formations were observed on the surface of silica.

DSC data confirmed the presence of stearic acid within SYLOID pores and the crystal behaviour of formulations with stearic acid amounts exceeding 100 % w/w, where needle-like formations were observed using SEM. However, the endothermic event in DSC for formulations containing 80 % stearic acid w/w and less was not confirmed to be crystal-related. Therefore, XRD analysis was used for further clarification of solid-state properties.

As seen in Fig. 8 above, SYLOID had no Bragg peaks and presented a halo which is supported by literature considering its amorphous form [37]. Stearic acid diffractogram contained several Bragg peaks around 6°, 21°, and 36° confirming the crystal structure of the lipid. Additionally, the peak at 21° was associated with polymorph C [46], indicating stearic acid's crystal structure and supporting the data from DSC. Formulations containing stearic acid presented a reading with a halo, representing SYLOID [47]. Also, all SYLOID-stearic acid formulations presented a Bragg peak at 21°, indicating the presence of crystalline stearic acid in the formulations. This finding supported DSC results for formulations containing 100 and 120 %, indicating that the second peak in the thermogram represented the needle-like formations on the surface first observed via SEM. As for formulations containing (20—80 % stearic acid w/w), the peak indicated the presence of stearic acid crystals, and in this case, nanocrystals, which could have formed during the evaporation process. These crystals could have caused the endothermic event in DSC, even though they were not evident in SEM, considering the high sensitivity of XRD analysis. These previous findings confirmed the crystal structure of stearic acid and that the needle-like formations on the surface of silica particles were stearic acid crystals.

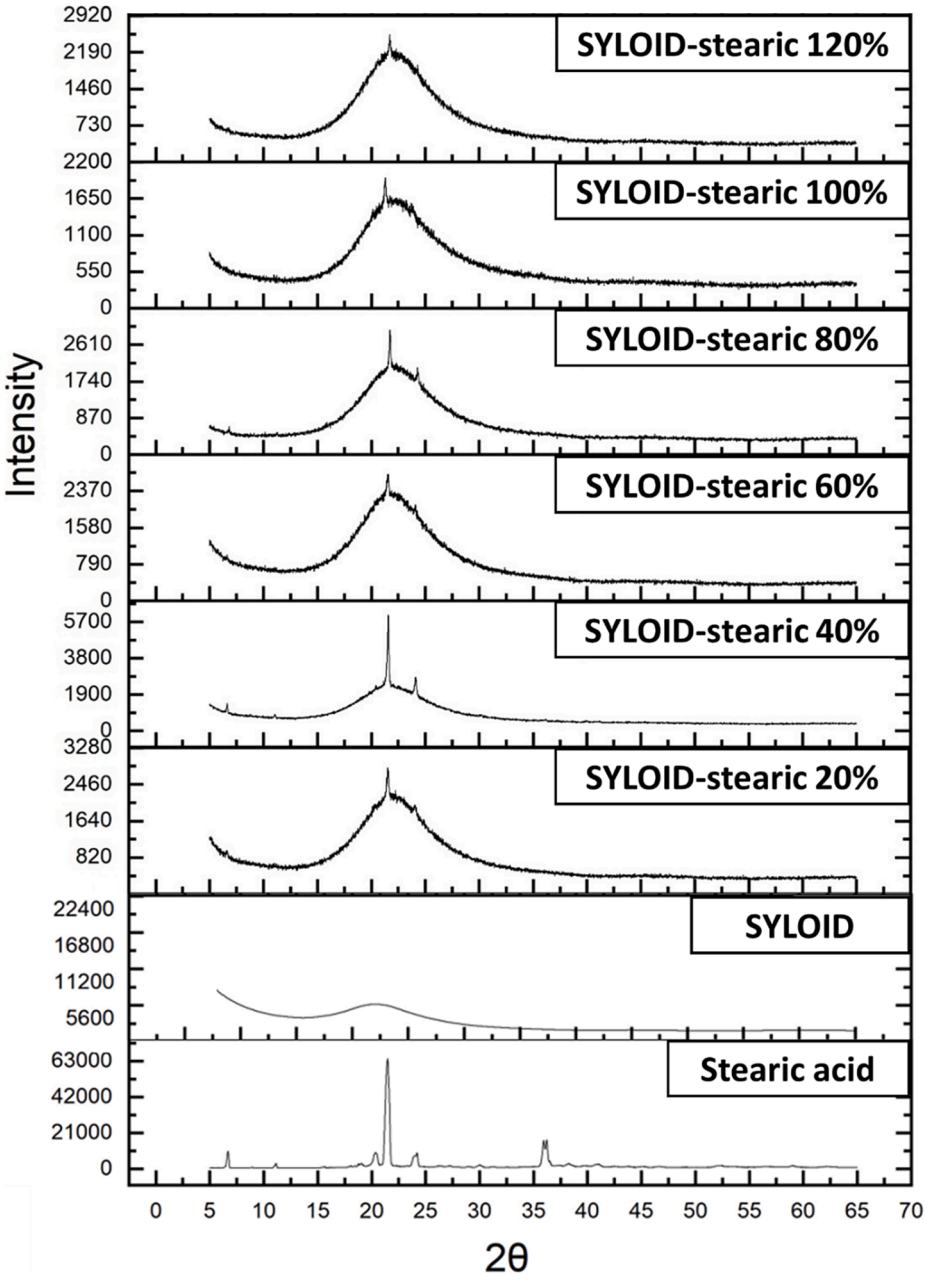

Fig. 8. XRD analysis for SYLOID-stearic acid formulations in different concentrations presenting the Bragg peaks associated with stearic acid crystal form.

Table 1
Surface area, pore volume, and pore size of SYLOID-stearic acid formulations in different concentrations.

Formulation	Surface area (m^2/g)	Pore volume (cc)	Pore size (nm)
SYLOID XDP 3050	340.44	2.10	15.49
SYLOID-stearic 20 % w/w	229.90	1.99	13.15
SYLOID-stearic 40 % w/w	215.08	1.48	13.13
SYLOID-stearic 60 % w/w	210.19	1.46	12.87
SYLOID-stearic 80 % w/w	168.54	1.12	12.75
SYLOID-stearic 100 % w/w	93.19	0.62	12.27
SYLOID-stearic 120 % w/w	93.26	0.59	12.01

3.6. Surface area and pore volume

Nitrogen porosimetry was utilised to assess the surface area, pore volume, and pore size of SYLOID-stearic acid formulations and to examine how increasing the stearic acid amount would affect them.

SYLOID XDP is a non-ordered mesoporous silica carrier that presented the surface area and pore volume of 340.44 m^2/g and 2.1 cc, respectively. As seen from Table 1 above, the increase in stearic acid loading led to a decrease in the surface area, pore volume, and pore size of the carrier due to the occupation of the mesoporous channels inside the porous matrix with stearic acid molecules [29]. This indicated that stearic acid populated the pores and covered the surface of silica. Moreover, the decrease in the surface area upon using 20 % stearic acid aligned with the calculated amount of stearic acid to cover the carrier surface in a monolayer (25.91 %). The pore volume of SYLOID-stearic 20 % was lower than SYLOID's, but not as other formulations, which indicated that stearic acid has only partially incorporated the porous

structure. Furthermore, the pore volume and surface area of SYLOID-stearic formulations decreased as stearic acid concentration increased, indicating that the pores of SYLOID were being filled with stearic acid, and the surface was covered. The same observation applied to the pore size as it decreased with the stearic acid increase due to the latter's capping of SYLOID's pores. This was further supported by SEM (Figs. 2 and 3), as well as confocal imaging (Fig. 6 a-f). In addition, the lowest pore volume surface area and pore size values were associated with the formulation containing 120 % stearic acid, which was related to stearic acid needle-like structures crystalising on the surface.

4. Conclusion

We reported the development of a mesoporous silica-lipid hybrid carrier using SYLOID XDP 3050 and stearic acid via ethanol evaporation in ascending concentrations (20–120 % w/w) as a novel approach for oral delivery. SEM analysis revealed increased pore capping with higher stearic acid concentrations, where above 80 %, needle-like structures formed on the silica surface due to stearic acid crystallisation. The size of the hybrid carrier increased with more stearic acid, as shown by laser diffraction. FTIR confirmed stearic acid inside the silica carrier through the detection of the carboxylic group, while confocal microscopy supported the presence of needle-like structures via autofluorescence. DSC identified stearic acid in two states, and a second melting peak was evident at concentrations above 80 % due to the melting of surface needle-like structures. XRD analysis confirmed the crystalline nature of stearic acid within the carrier. Nitrogen porosimetry demonstrated that pore volume, surface area, and pore size decreased with higher stearic acid amounts, with the lowest values at 120 % w/w (0.59 cc). This newly developed SYLOID-stearic acid carrier will now be used for peptide delivery as future work will focus on using this platform for enhancing protein oral delivery.

CRediT authorship contribution statement

Mohamad Anas Al Tahan: Writing – original draft, Methodology, Formal analysis, Data curation. **Ali Al-Khattawi:** Writing – review & editing, Supervision, Project administration, Conceptualization. **Craig Russell:** Writing – review & editing, Supervision.

Declaration of Competing Interest

The authors declare that they have no known competing financial interests or personal relationships that could have appeared to influence the work reported in this paper.

Acknowledgements

The authors would like to thank Grace W.R for kindly providing the mesoporous silica carrier (SYLOID XDP 3050).

Funding

This research did not receive any specific grant from funding agencies in the public, commercial, or not-for-profit sectors.

Data availability

Data will be made available on request.

References

[1] A. Lerida-Viso, A. Estepa-Fernandez, A. Garcia-Fernandez, V. Marti-Centelles, R. Martinez-Manez, Biosafety of mesoporous silica nanoparticles; towards clinical translation, Adv Drug Deliv Rev 201 (2023), https://doi.org/10.1016/j.addr.2023.115049.

[2] M.A. Al Tahan, S. Al Tahan, Pioneering advances and innovative applications of mesoporous carriers for mitochondria-targeted therapeutics, Br. J. Biomed. Sci. 81 (2024), https://doi.org/10.3389/bjbs.2024.13707.

[3] S.R. Pamshong, D. Bhatane, S. Sarnaik, A. Alexander, Mesoporous silica nanoparticles: An emerging approach in overcoming the challenges with oral delivery of proteins and peptides, *Colloids Surf B Biointerfaces* 232 (2023) 113613, https://doi.org/10.1016/j.colsurfb.2023.113613.

[4] A. Bouamrani, Y. Hu, E. Tasciotti, L. Li, C. Chiappini, X. Liu, M. Ferrari, Mesoporous silica chips for selective enrichment and stabilization of low molecular weight proteome, *Proteomics* 10 (3) (Feb 2010) 496–505, https://doi.org/10.1002/pmic.200900346.

[5] S. Kheirkhah, M. Abedi, F. Zare, M. Salmanpour, S.S. Abolmaali, A.M. Tamaddon, Surface engineered palmitoyl-mesoporous silica nanoparticles with supported lipid bilayer coatings for high-capacity loading and prolonged release of dexamethasone: A factorial design approach, *J. Drug Delivery Sci. Technol.* 78 (2022), https://doi.org/10.1016/j.jddst.2022.103943.

[6] J. Gupta, M. Quadros, M. Momin, Mesoporous silica nanoparticles: Synthesis and multifaceted functionalization for controlled drug delivery, *J. Drug Delivery Sci. Technol.* 81 (2023), https://doi.org/10.1016/j.jddst.2023.104305.

[7] D. Cai, C. Han, C. Liu, X. Ma, J. Qian, J. Zhou, Y. Li, Y. Sun, C. Zhang, W. Zhu, Chitosan-capped enzyme-responsive hollow mesoporous silica nanoplatforms for colon-specific drug delivery, Nanoscale Res Lett 15 (1) (2020) 123, https://doi.org/10.1186/s11671-020-03351-8.

[8] F. Ahmadi, A. Sodagar-Taleghani, P. Ebrahimnejad, S. Pouya Hadipour Moghaddam, F. Ebrahimnejad, K. Asare-Addo, A. Nokhodchi, A review on the latest developments of mesoporous silica nanoparticles as a promising platform for diagnosis and treatment of cancer, Int J Pharm 625 (2022) 122099, https://doi.org/10.1016/j.ijpharm.2022.122099.

[9] A. Bakhshian Nik, H. Zare, S. Razavi, H. Mohammadi, P. Torab Ahmadi, N. Yazdani, M. Bayandori, N. Rabiee, J. Izadi Mobarakeh, Smart drug delivery: Capping strategies for mesoporous silica nanoparticles, Microporous Mesoporous Mater. 299 (2020), https://doi.org/10.1016/j.micromeso.2020.110115.

[10] J. Zhu, Y. Zhang, X. Chen, Y. Zhang, K. Zhang, H. Zheng, Y. Wei, H. Zheng, J. Zhu, F. Wu, J.G. Piao, Z. Zhu, F. Li, Angiopep-2 modified lipid-coated mesoporous silica nanoparticles for glioma targeting therapy overcoming BBB, *Biochem Biophys Res Commun* 534 (2021) 902–907, https://doi.org/10.1016/j.bbrc.2020.10.076.

[11] C. Dong, X. Zhang, H. Cai, C. Cao, K. Zhou, X. Wang, X. Xiao, Synthesis of stearic acid-stabilized silver nanoparticles in aqueous solution, *Adv. Powder Technol.* 27 (6) (2016) 2416–2423, https://doi.org/10.1016/j.apt.2016.08.018.

[12] Z. Negahban, S.A. Shojaosadati, S. Hamedi, A novel self-assembled micelles based on stearic acid modified schizophyllan for efficient delivery of paclitaxel, *Colloids Surf B Biointerfaces* 199 (Mar 2021) 111524, https://doi.org/10.1016/j.colsurfb.2020.111524.

[13] A. Patti, H. Lecocq, A. Serghei, D. Acierno, P. Cassagnau, The universal usefulness of stearic acid as surface modifier: applications to the polymer formulations and composite processing, *J. Ind. Eng. Chem.* 96 (2021) 1–33, https://doi.org/10.1016/j.jiec.2021.01.024.

[14] K. Ajito, M. Nakamura, T. Tajima, and Y. Ueno, "Terahertz Spectroscopy Methods and Instrumentation," 2016.

[15] B. Calvo, E.A. Cepeda, Solubilities of stearic acid in organic solvents and in azeotropic solvent mixtures, *J. Chem. Eng. Data* 53 (3) (2008) 628–633, https://doi.org/10.1021/je7006567.

[16] W. Beckmann, R. Boistelle, K. Sato, Solubility of the A, B, and C polymorphs of stearic acid in decane, methanol, and butanone, *J. Chem. Eng. Data* 29 (2) (1984) 211–214, https://doi.org/10.1021/je00036a034.

[17] B. Zhou, L. Zhen, Y. Yang, W. Ma, Y. Fu, X. Duan, H. Wang, Novel composite phase change material of high heat storage and photothermal conversion ability, *J. Storage Mater.* 49 (2022), https://doi.org/10.1016/j.est.2022.104101.

[18] H. Yuan, X. Bao, Y.Z. Du, J. You, F.Q. Hu, Preparation and evaluation of SiO2-deposited stearic acid-g-chitosan nanoparticles for doxorubicin delivery, *Int J Nanomedicine* 7 (2012) 5119–5128, https://doi.org/10.2147/IJN.S35575.

[19] T. Kadoono, M. Ogura, Heat storage properties of organic phase-change materials confined in the nanospace of mesoporous SBA-15 and CMK-3, *Phys Chem Chem Phys* 16 (12) (2014) 5495–5498, https://doi.org/10.1039/c3cp55429e.

[20] R.A. Mitran, D. Berger, C. Matei, Phase change materials based on mesoporous silica, *Curr. Org. Chem.* 22 (27) (2019) 2644–2663, https://doi.org/10.2174/1385272822666180827125651.

[21] Y. Gao, Y. He, H. Zhang, Y. Zhang, T. Gao, J.H. Wang, S. Wang, Zwitterion-functionalized mesoporous silica nanoparticles for enhancing oral delivery of protein drugs by overcoming multiple gastrointestinal barriers, J Colloid Interface Sci 582 (Pt A) (2021) 364–375, https://doi.org/10.1016/j.jcis.2020.08.010.

[22] B.D. Almquist, N.A. Melosh, Fusion of biomimetic stealth probes into lipid bilayer cores, *Proc Natl Acad Sci U S A* 107 (13) (2010) 5815–5820, https://doi.org/10.1073/pnas.0909250107.

[23] M. Lengyel, N. Kállai-Szabó, V. Antal, A.J. Laki, I. Antal, Microparticles, microspheres, and microcapsules for advanced drug delivery, Sci. Pharm. 87 (3) (2019), https://doi.org/10.3390/scipharm87030020.

[24] T. Desai, L.D. Shea, Advances in islet encapsulation technologies, *Nat Rev Drug Discov* 16 (5) (2017) 338–350, https://doi.org/10.1038/nrd.2016.232.

[25] S. Solomon, J. Iqbal, A.B. Albadarin, Insights into the ameliorating ability of mesoporous silica in modulating drug release in ternary amorphous solid dispersion prepared by hot melt extrusion, *Eur J Pharm Biopharm* 165 (2021) 244–258, https://doi.org/10.1016/j.ejpb.2021.04.017.

[26] S. Fan, H. Gao, W. Dong, J. Tang, J. Wang, M. Yang, G. Wang, Shape-stabilized phase change materials based on stearic acid and mesoporous hollow SiO2

microspheres (SA/SiO2) for thermal energy storage, *Eur. J. Inorg. Chem.* 2017 (14) (2017) 2138–2143, https://doi.org/10.1002/ejic.201601380.
[27] C.G. Bavnhoj, M.M. Knopp, C.M. Madsen, K. Lobmann, The role interplay between mesoporous silica pore volume and surface area and their effect on drug loading capacity, *Int J Pharm X* 1 (2019) 100008, https://doi.org/10.1016/j.ijpx.2019.100008.
[28] T.J. Dening, L.S. Taylor, Supersaturation Potential of Ordered Mesoporous Silica Delivery Systems. Part 1: Dissolution Performance and Drug Membrane Transport Rates, *Mol Pharm* 15 (8) (2018) 3489–3501, https://doi.org/10.1021/acs.molpharmaceut.8b00488.
[29] S. Hong, S. Shen, D.C. Tan, W.K. Ng, X. Liu, L.S. Chia, A.W. Irwan, R. Tan, S. A. Nowak, K. Marsh, R. Gokhale, High drug load, stable, manufacturable and bioavailable fenofibrate formulations in mesoporous silica: a comparison of spray drying versus solvent impregnation methods, *Drug Deliv* 23 (1) (2016) 316–327, https://doi.org/10.3109/10717544.2014.913323.
[30] M. Kruk, M. Jaroniec, A. Sayari, Application of large pore MCM-41 molecular sieves to improve pore size analysis using nitrogen adsorption measurements, *Langmuir* 13 (23) (1997) 6267–6273, https://doi.org/10.1021/la970776m.
[31] J. Schindelin, I. Arganda-Carreras, E. Frise, V. Kaynig, M. Longair, T. Pietzsch, S. Preibisch, C. Rueden, S. Saalfeld, B. Schmid, J.Y. Tinevez, D.J. White, V. Hartenstein, K. Eliceiri, P. Tomancak, A. Cardona, Fiji: an open-source platform for biological-image analysis, *Nat Methods* 9 (7) (2012) 676–682, https://doi.org/10.1038/nmeth.2019.
[32] B. Vranikova, A. Niederquell, F. Ditzinger, Z. Sklubalova, M. Kuentz, Mechanistic aspects of drug loading in liquisolid systems with hydrophilic lipid-based mixtures, Int J Pharm 578 (2020) 119099, https://doi.org/10.1016/j.ijpharm.2020.119099.
[33] L. Huo, X. Han, L. Zhang, B. Liu, R. Gao, B. Cao, W.-W. Wang, C.-J. Jia, K. Liu, J. Liu, J. Zhang, Spatial confinement and electron transfer moderating Mo N bond strength for superior ammonia decomposition catalysis, *Appl Catal B* 294 (2021), https://doi.org/10.1016/j.apcatb.2021.120254.
[34] C. Blach, A.J. Gravelle, F. Peyronel, J. Weiss, S. Barbut, A.G. Marangoni, Revisiting the crystallization behavior of stearyl alcohol : stearic acid (SO : SA) mixtures in edible oil, *RSC Adv.* 6 (84) (2016) 81151–81163, https://doi.org/10.1039/c6ra15142f.
[35] V. Malta, G. Celotti, R. Zannetti, A.F. Martelli, Crystal structure of the C form of stearic acid, *J. Chem. Soc. B* (1971), https://doi.org/10.1039/j29710000548.
[36] C. Charnay, S. Begu, C. Tourne-Peteilh, L. Nicole, D.A. Lerner, J.M. Devoisselle, Inclusion of ibuprofen in mesoporous templated silica: drug loading and release property, *Eur J Pharm Biopharm* 57 (3) (2004) 533–540, https://doi.org/10.1016/j.ejpb.2003.12.007.
[37] A. Baan, P. Adriaensens, J. Lammens, R. Delgado Hernandez, W. Vanden Berghe, L. Pieters, C. Vervaet, F. Kiekens, Dry amorphisation of mangiferin, a poorly water-soluble compound, using mesoporous silica, Eur J Pharm Biopharm 141 (2019) 172–179, https://doi.org/10.1016/j.ejpb.2019.05.026.
[38] A.C. Teixeira, A.C. Fernandes, A.R. Garcia, L.M. Ilharco, P. Brogueira, A. M. Goncalves da Silva, Microdomains in mixed monolayers of oleanolic and stearic acids: thermodynamic study and BAM observation at the air-water interface and AFM and FTIR analysis of LB monolayers, Chem Phys Lipids 149 (1–2) (2007) 1–13, https://doi.org/10.1016/j.chemphyslip.2007.05.004.
[39] M.A. Al Tahan, K. Michaelides, S. Somasekharan Nair, S. AlShatti, C. Russell, A. Al-Khattawi, Mesoporous silica microparticle-protein complexes: effects of protein size and solvent properties on diffusion and loading efficiency, Br. J. Biomed. Sci. 81 (2024), https://doi.org/10.3389/bjbs.2024.13595.
[40] A.N. Semenov, B.P. Yakimov, A.A. Rubekina, D.A. Gorin, V.P. Drachev, M. P. Zarubin, A.N. Velikanov, J. Lademann, V.V. Fadeev, A.V. Priezzhev, M. E. Darvin, E.A. Shirshin, The Oxidation-Induced Autofluorescence Hypothesis: Red Edge Excitation and Implications for Metabolic Imaging, Molecules 25 (8) (2020), https://doi.org/10.3390/molecules25081863.
[41] S.S. Sagiri, V.K. Singh, K. Pal, I. Banerjee, P. Basak, Stearic acid based oleogels: a study on the molecular, thermal and mechanical properties, *Mater Sci Eng C Mater Biol Appl* 48 (Mar 2015) 688–699, https://doi.org/10.1016/j.msec.2014.12.018.
[42] Y. Zhou, J. Wang, Y. Xiao, T. Wang, X. Huang, The Effects of Polymorphism on Physicochemical Properties and Pharmacodynamics of Solid Drugs, *Curr Pharm Des* 24 (21) (2018) 2375–2382, https://doi.org/10.2174/1381612824666180515155425.
[43] S. Zhu, P.D. Pudney, M. Heppenstall-Butler, M.F. Butler, D. Ferdinando, M. Kirkland, Interaction of the acid soap of triethanolamine stearate and stearic acid with water, *J Phys Chem B* 111 (5) (2007) 1016–1024, https://doi.org/10.1021/jp0659047.
[44] Y. Lin, C. Zhu, G. Fang, Synthesis and properties of microencapsulated stearic acid/silica composites with graphene oxide for improving thermal conductivity as novel solar thermal storage materials, *Sol. Energy Mater. Sol. Cells* 189 (2019) 197–205, https://doi.org/10.1016/j.solmat.2018.10.005.
[45] T.T. Le, A.K. Elzhry Elyafi, A.R. Mohammed, A. Al-Khattawi, Delivery of poorly soluble drugs via mesoporous silica: impact of drug overloading on release and thermal profiles, Pharmaceutics 11 (6) (2019), https://doi.org/10.3390/pharmaceutics11060269.
[46] N. Garti, E. Wellner, S. Sarig, Stearic acid polymorphs in correlation with crystallization conditions and solvents, *Krist. Tech.* 15 (11) (1980) 1303–1310, https://doi.org/10.1002/crat.19800151112.
[47] B. Vranikova, A. Niederquell, Z. Sklubalova, M. Kuentz, Relevance of the theoretical critical pore radius in mesoporous silica for fast crystallizing drugs, Int J Pharm 591 (2020) 120019, https://doi.org/10.1016/j.ijpharm.2020.120019.